10th International Symposium on the Science and Processing of Cast Iron – SPCI10

Metallographic investigation of Nd: YAG laser processed ductile iron surfaces

A. Nofal*, H. El-Gazzar and M. Ibrahim
Department of Foundry Technology, Central Metallurgical R&D Institute, Cairo, Egypt

Ductile cast iron is finding increased applications in parts subjected to different types of wear due to sliding contact and hence novel hardening techniques of mating surfaces need to be investigated. Laser hardening has proved to be very effective in enhancing the tribological properties of ductile iron surface.
In this work, high power CW-Nd:YAG 600 W laser was used for the processing of ductile iron surfaces at different scanning speeds. The depth and hardness of the processed surface were found to be dependent on the scanning speed. At lower speeds of 25 cm/min, remelting and rapidly solidified layer resulted in the formation of carbidic and graphite free surface layer of microhardness around 1200 HV. Increasing the scanning speed to 125 cm/min results in heating of the surface layer to the austenitic region with the formation of martensitic layer upon rapid cooling.
Some microstructural features associated with the laser processing were noticed at the hardened/HAZ transition layer and suggestions were made for their formation. Microhardness profile across the hardened zone were plotted, where different scanning speeds were shown to affect the hardened case depth and hardness.

Keywords: ductile iron, laser processing, surface hardening, surface remitting, accelerated graphitization, microhardness profile.

Introduction

Ductile cast irons are still finding increasing applications in many industrial sectors, thanks to their good mechanical properties, excellent castability and machinability, high thermal conductivity as excellent noise and vibration damping capacity as well as reasonable price. The strength, wear and fatigue properties of ductile irons can be improved by means of different conventional surface treatments such as induction and flame hardening and more recently by electron beam and laser technologies. However, the laser surface hardening stands out for a number of reasons, some of them are:

- Possibility of accurate control the area where laser radiation should be delivered, as well as the amount and rate of energy deposition. The laser beam is finite in size; therefore, the process is ideally suited to conduct specific localized area treatment.
- The heated thin surface layers do not require external quenching since the bulk of the material serves as a thermal sink.
- Due to the small energy input received by the material, distortion of the treated components may be minimized or eliminated, rendering the final machining or refinishing unnecessary.

Laser processing is used to produce through rapid heating and cooling a thin hard layer on the surface of a bulk material, with enhanced abrasion and corrosion resistance. Both surface hardening and melting have been used to impart better tribological properties to the surface of grey and ductile iron.

Recently a comprehensive state-of-the-art of laser processing for material surface modification has been published[1], indicating that lasers provide unlimited possibilities for surface engineering, such as solid state hardening, melting, alloying, cladding, ablation, shot peening, cleaning and texturing.

In a recent investigation[2], solid-state phase transformation during the laser surface hardening of grey cast iron was induced using low power fiber laser of power 100 W in both continuous as well as pulsed modes in conjunction with a beam-integrator. The effect of process parameters, e.g. beam power, beam diameter, travel speed and bulk time on the geometry, dimensions and hardness of heat affected zone was studied. Application of low-power lasers was shown to be more favorable compared to expensive large-sized powerful CO_2 or Nd:YAG lasers usually used as the low power thermal process avoids post process machining with minimum distortion.

Evaluation of the Nd:YAG bulked laser surface hardening of cast iron used in automotive industry was reviewed[3].

Matsuyama and Shibata[4] reported in an earlier investigation that in the laser surface processed ferritic ductile iron, graphite spheroids were surrounded by a martensitic ring, which resulted in considerable increase in wear resistance, proportional to the amount of martensite in the matrix. On the other hand, the impact strength of laser processed iron

* Corresponding author, email: adelnofal@hotmail.com

was inferior to that of untreated ductile iron. However, the impact strength of the laser treated iron with a ferritic matrix was superior to that of untreated iron with a pearlitic matrix.

Chen et al[5,6] have studied the effect of LSM process parameter on the microstructure, hardness and wear resistance of ductile iron. The refined austenitic microstructure produced by LSM could induce better wear resistance as a result of deformation induced martensitic transformation. However, such phase transformation may develop microcracks at the martensitic-austenitic interface due to the volume change involved in austenite to martensite transformation and the deformation constraints at these interfaces.

In a recent work, Fernández-Vicente et al[7] have analysed the microstructures obtained from LSM and LSH of ductile iron of different compositions under different laser processing conditions. The mechanism explaining the formation of cracks during laser treatment was studied. Extensive cracking of the laser processed layer was related to thermal stresses generated under high-energy density conditions as well as to transformational stresses associated with retained austenite contents exceeding 40%.

Farias et al[8] in an attempt to find out the laser operating parameters which will lead to certain desired properties associated with laser surface hardening, conducted the metallurgical analysis, the thermodilatometric characterization of structural evolution during rapid heating and cooling involved in LSH together with microstructural analysis of laser treated specimens for ductile cast iron as well as plain carbon steel XC42.

Wang and Bergmann[9,10] have utilized LSM to improve the abrasion resistance of ductile iron by generating a rapidly solidified ultra-fine ledeburitic surface layer. A novel iron-base material containing both the rapidly solidified eutectic cementite and the ultra-fine graphite nodules could be produced by partial graphitization of the cementite. This material was expected to have excellent performance under dry or boundary lubrication wear conditions due to its combination of the excellent abrasion resistance of the rapidly solidified eutectic cementite and the superior self-lubrication, heat conducting and damping properties of the graphitic phase.

The effect of processing parameters (beam-substrate interaction time and power density) during laser surface processing of ductile iron was earlier studied.[11,12]. The microstructure of the melted zone depends mainly on the its solidification rate and two different microstructures were obtained; at lower solidification rate a dendritic microstructure with low hardness and a second with lamellar ferrite plus parallel cementite plates with high hardness at high solidification rate. Chen et al[12] proposed that excessive supercooling of the melt during laser processing can reduce the nucleation level in the molten iron, thus enhancing the undercooling during solidification leading to the formation of carbides.

Grum and Štrum[13-15] used a mathematical model to determine the temperature cycles in grey and ductile irons and the depth of the modified layer. The mathematically obtained results were critically assessed and compared with the experimental results. The optimum laser melt-hardening conditions for individual parts were determined with a reduced number of trial experiments.

Using 500 W Nd:YAG laser equipped with self-designed diffractive optical element, a novel surface layer having both rapidly solidified eutectic cementite, martensite and graphite particle was obtained on the surface of pearlite-ferrite matrix ductile iron. The microstructure along the layer surface and the layer depth had obvious gradient distribution consisting of fine austenite, martensite with residual austenite and deudritic austenite growing radially along the periphery of graphite, martensite with residual austenite and ledeburite shell around the graphite nodules.[16]

The erosion resistance of the laser treated ductile iron was claimed to be 110 times greater that the untreated material.[17] The erosion mechanism of the untreated ductile iron under normal and oblique angles was by severe plastic deformation and ploughing; whilst the treated material was eroded by fatigue cracking. The enhanced erosion resistance after laser treatment was related to the very fine structure, high microhardness (650 Hv0.1) with the resistance to plastic flow and to the dissolution of the graphite nodules.

Recently, it was reported that the matrix of the as-cvast ductile iron specimens shows three stages of wear[18]: mild, transition and severe, while the laser processed specimens show only two stages of wear: mild and transition. The increased wear resistance was related to fine microstructures, work hardening as well as stress induced phase transformation of retained austenite to martensite.

Throughout the abovementioned reports, a very wide spectrum of microstructures has been observed and used to explain different surface hardness values, microhardness profiles across the transverse sections of the treated samples, abrasion resistance as well as the tendency of the treated surface to develop cracks.

This paper reports the first results of a research project aiming at investigating the microstructural features of ductile iron (DI) and austempered ductile iron (ADI) subjected to Nd:YAG laser surface treatment using different power intensities at scanning speeds. The results shown are limited to ductile iron treated with one power intensity of 600 W and scanning speeds from 25 to 125 cm/min.

Experimental Procedure

The ductile iron and ADI used throughout this work was melted in 100 kg MF induction furnace to reach the nominal chemical composition of 3.6%C, 2%Si, 0.3%Mn, 0.01%S.

The molten iron was treated with 10% Mg FeSiMg alloy in a Vortex unit, inoculated with foundry grade ferrosilicon and poured in Y-blocks of 200*100*15 mm^3 dimensions. Rectangular specimens of 100*10*15 mm^3 were machined from the ductile iron stock. The microstructure of DI before subjecting to laser processing was ferrite/pearlitic.

Laser treatment was performed using a high-power (2 kW) diode pumped Nd-YAG laser (Rofin Sinar DY 022) in CW mode, equipped with a 3-axis computer numerical controlled work table and a 6-axis robot was used to process the DI specimens. The DI samples were processed with 600 W laser beam at scanning speeds of 25, 75 and 125 cm/min. Multipass overlap treatment was carried out, with overlap ratio of about 15%. The overlap ratio is defined as xxxx (L/W) x 100 pct, where L is the overlap width, i.e. the width which the succeeding processing track overlaps on the preceding processed track, and W is the width of the single processing track.

The incident laser beam was focused to a spot with a diameter of 3 mm. During laser processing, the sample surface was protected by argon gas (1 bar).

Microstructural analyses were carried out using both optical as well as scanning electron microscopy (SEM). Metallographic samples in the transverse section of the laser processed track were prepared using conventional metallographic techniques, then etched with 2 pct nital. The depth of the processed zone was measured using an optical microscope on as-polished surface for higher accuracy.

The hardness of the upper surface of the processed zone was measured at 0.1 mm below the irradiated surface. The microhardness profiles on transverse sections were measured and plotted as a function of the distance from the irradiated surface.

Results and Discussion

Microstructure of DI Processed with 600 W Laser

The microstructure of the DI irradiated with 600 W and scanned at 25 m/min speed laser beam is shown in Fig.1 at low magnification. The microstructure is homogeneous and free of any graphite nodules. The laser processed zone is of semicircular morphology due to the Gaussian distribution of incident power across the diameter.

This figure shows the variation of the case depth in a transverse section perpendicular to the laser treated surface and lasing direction as a function of laser scanning speed at 600 W power intensity. It is obvious that the higher the speed, the smaller the corresponding interaction time for laser-material interaction and hence the lower value of the case depth. SEM micrograph shown in Fig.2 reveals that the microstructure consists of eutectic lamellar carbides (cementite) and a mixed matrix of martensite and retained austenite. The eutectic structure is an indication of surface remelting, the molten metal pool will solidify under severe cooling rate, caused by the chilling effect of the underlying solid metal which acts as very powerful heat sink.

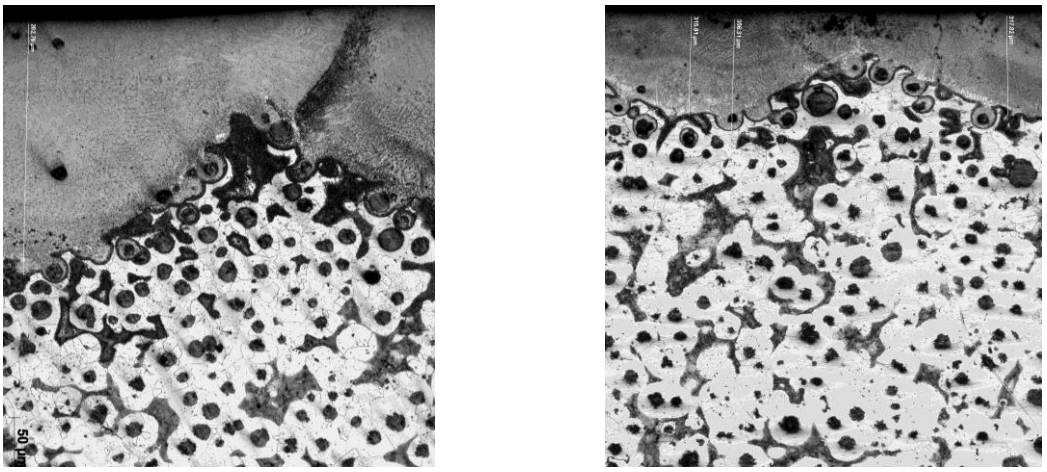

(a) (b)

Fig.1: microstructures of hardened layer of DI treated with 600 W laser at scanning speeds of a) 25 cm/min, b) 75 cm/min

Fig. 1-a shows that under the overlays, the volume fraction of cementite, which is the white etching phase, was significantly reduced after the overlap reheating by the subsequent track and the former rapidly solidified cementite almost decomposed.

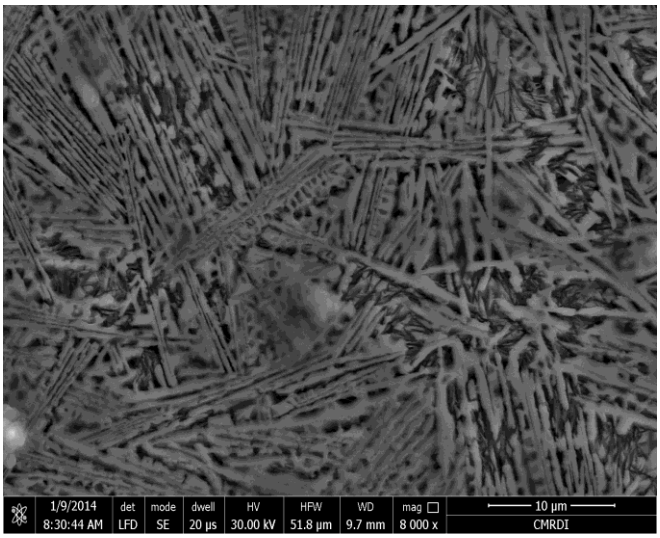

Fig.2: SEM micrograph of the remelted layer of DI processed by 600 W at scanning speed of 25 cm/min

SEM examination (Fig.3) reveals that the formerly solidified carbides had transformed into extremely fine graphite particles of approximately 1-2 μm in diameter with the formed austenite transformed on subsequent rapid cooling into martensite and retained austenite. The degree of graphitization seems to be maximum and decreases with the distance from the overlap lower surface. The graphitization almost disappears at 60-70 μm from the overlap boundary and the matrix is only tempered without any noticeable degree of graphitization. Careful examination of SEM micrograph of the partially graphitized zone (Fig.3-b) shows that some undissolved carbide phase still exists and that the graphite particles are in contact with the undissolved cementite. This may give indication that the cementite-matrix interfaces are preferential sites for the cementite-graphite phase transformation. Such accelerated graphitization of carbides may be related to different factors:

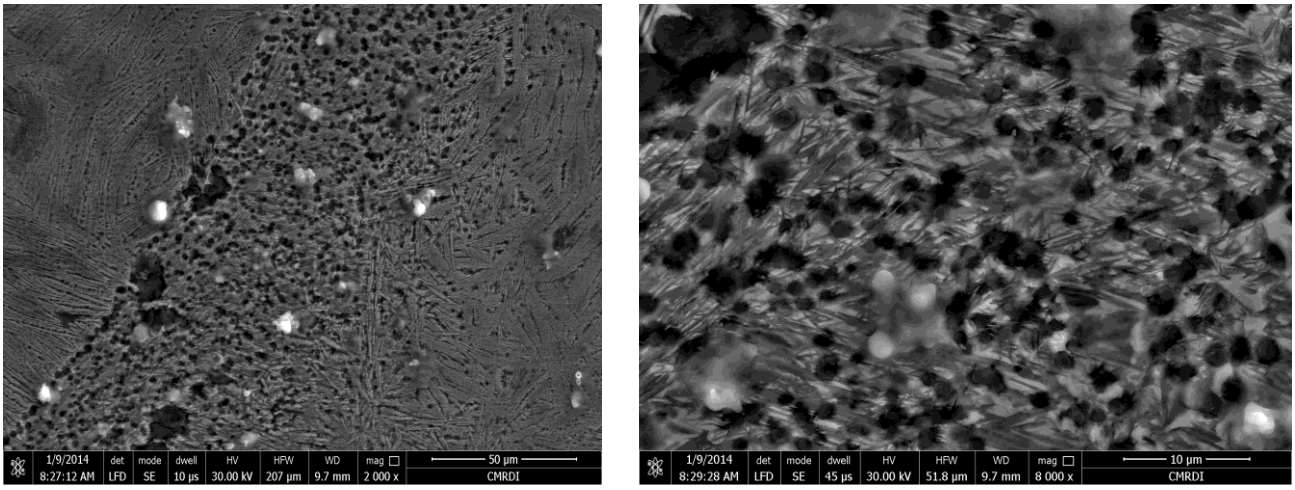

(a) (b)

Fig.3: microstructure of the overlap boundary layer showing the ultrafine graphite nodules precipitation
a) at lower magnification, b) at higher magnification

- Thermodynamic factors related to the composition of the iron, the relatively high C and Si contents, both are potent graphiting elements that are not usual for white iron composition, would significantly increase the graphitization potential of the iron and would, at least partly contribute to the unusually accelerated graphitization process in the laser remelted ductile iron.
- Kinetic factors related to the ultrafine structure of the microstructure of extremely rapidly solidified laser remelted pool. Such structure would provide enormous cementite-matrix interfaces, which are favorite heterogeneous nucleation sites for graphite. Moreover, the very short C-difusion path in such ultrafine structure would enhance the graphitization process.

- The extremely rapid solidification, and the resulting ultrafine structure, remarkably increase the density of crystal defects such as vacancies, dislocation, etc .. at the carbide/matrix interface, which would decrease the activation energy required for the graphite nucleation at those sites.
- Another mechanism has been earlier proposed[9], where pulsed Nd:YAG laser beam was used for remelting, the accelerated graphitization was related to the unique heating behavior of the pulsed laser beam to material. Such mechanism was quantitatively demonstrated based on simplified calculations of temperature profiles during pulsed Nd:YAG laser beam scanning. It was shown that temperature fluctuates very violently, with each cycle of temperature fluctuation regarded as a microannealing treatment, enhancing the cementite dissolution and the acceleration of ultrafine graphite nucleation. However, in our investigation, CW-mode of laser was used, hence, this mechanism may be excluded when considering reasons behind the precipitation of the ultrafine graphite nodules beneath the overlap boundary.

It is of interest to notice from Fig.1 that the graphitization zone disappeared when increasing the scanning speed, which indicates that at higher speeds, the heat input at the overlap is not sufficient to induce significant graphitization of carbides.

Fig. 4 shows the microstructure of the interface between the remelted zone and the substrate, i.e. the upper part of the heat-affected zone (HAZ). The temperature reached in this zone was not high enough to dissolve all graphite nodules and some nodules are still noticed surrounded by a matrix of plate martensite and retained austenite. The dendritic morphology of the solid/liquid interface of austenite suggests that the solidification velocity was rather high. It has been reported that with increasing the solidification rate of the laser remelted Fe-C-Si alloys, the austenite growth morphology would transform from planar to cellular to dendritic[19].

Fig.4: microstructure at the upper part of the HAZ or transition zone

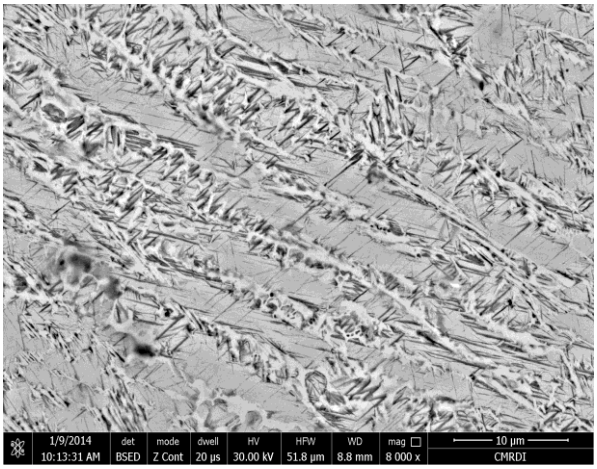

Fig.5: microstructure of the hardened layer using 600 W laser with scanning speed of 125 cm/min

Effect of Laser Scanning Speed

The microstructure of the surface processed zone considerably changes with increasing the scanning speed. Higher scanning speeds mean lower heat input received by the sample surface hence, lower probability of surface remelting and the subsequent formation of ledeburitic structure in the hardened layer. Fig.5 shows SEM micrographs of the surface layers of samples processed with scanning speeds of 125 cm/min. It seems that at the high scanning speed of 125 cm/min the heat input was not enough to remelt the sample surface which was only heated to the austenitic zone with the subsequent transformation of the austenitic dendrites to martensite as shown in Fig.5.

Moreover, in the samples processed with the lowest heat input at scanning speed of 125 cm/min, two interesting features have been noticed:

i) The substrate in the vicinity of the bottom of the hardened zone (i.e. the upper part of the heat affected zone) is characterised by the appearance of coarse plate martensite, typical of high-C martensite, together with retained austenite Fig.6. This may be explained by the rejection of carbon atoms by the C-saturated austenite upon cooling, which may create a C-enriched layer at the interface between the hardened and the transition or heat-affected zones. The formation of such coarse plate martensite in that area has been reported before[9], but without explanation.
ii) The originally ferritic halos in the as-cast samples are transformed to two layers, an inside one near the graphite spheroid consisting of austenitic dendrites and an outer shell with martensitic structure, Fig.7. If the applied power induces sufficient heat, the carbon of the graphite nodules may dissolve in the adjacent layer of the austenitic shell, thus leading to increased C-content and stabilising the austenite upon subsequent rapid quenching of that layer, austenite dendrites may be seen at the internal halo around the graphite spheroids. The carbon diffusion from the

graphite spheroid would lower the liquidus temperature of the adjacent layer due to increased C-content, leading to incipient fusion of that layer with the high-C molten layer solidifying in the form of dendritic retained austenite.

The C-content of the outer layer of the austenitic shell around the graphite spheroid may be not so highly enriched with carbon to stabilise the austenite and subsequent quenching will transform into a martensitic layer as shown in Fig.7.

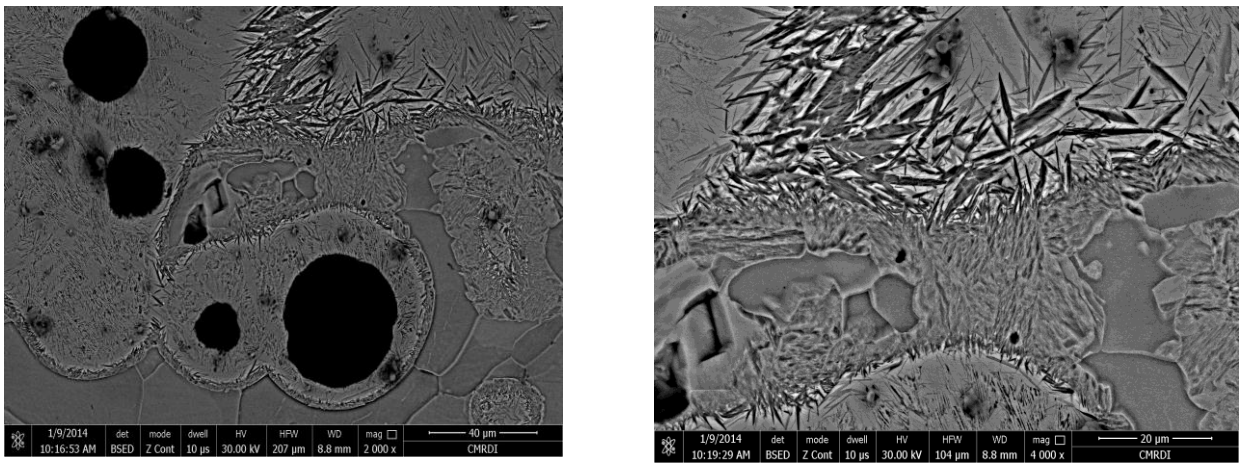

(a) (b)

Fig.6: Coarse martensite plates at the transition zone between the laser irradiated zone and the HAZ. a) at lower magnification, b) at higher magnification

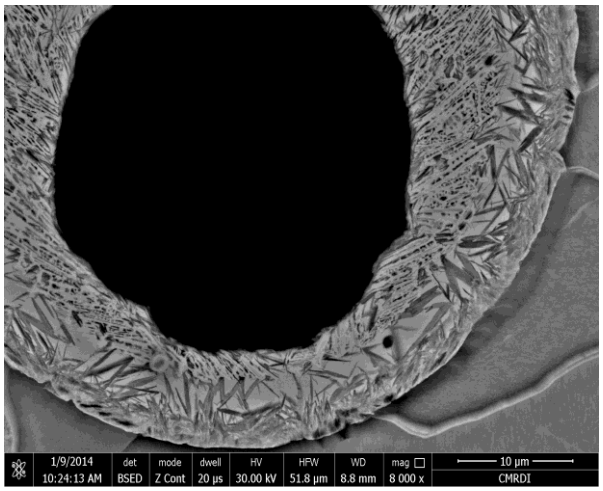

Fig.7: Outer shell around a graphite spheroid with an internal layer of austenitic dendrites and outer layer of martensite.

Microhardness Profile

As shown in Fig.1 and the microhardness profile of Fig.8, the thickness of the layer remelted and hardened zone decreases with increasing the laser scanning speed, apparently due to the lower heat input associated with higher scanning speeds.

The microhardness gradient from the sample surface to the lower part of the hardened zone drops more steeply with increasing the scanning speed. At 0.4 mm distance from the sample surface the microhardness drops from 1200 to 1000 to 400 HV when increasing g the scanning speed from 25 to 75 to 125 cm/min, respectively. Increased scanning speeds reduce both the thickness of the hardened layer as well as the hardness values achieved at fixed distance from the processed surface.

It should be noted that the surface hardness of that sample, processed at 600 W is around 960 HV, which is somewhat lower than the first recorded microhardness value at 0.2 mm beneath the melt surface, which may be related to slight surface decarburisation during remelting process.

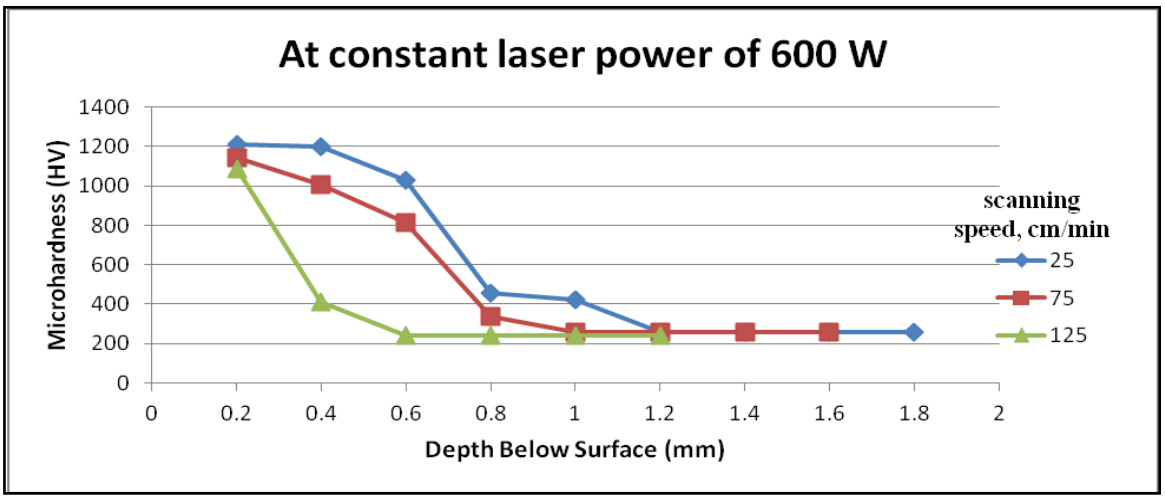

Fig8: Microhardness profile from the sample surface, as a function of scanning speed

Conclusions

1. The surface of ductile cast iron was processed with a high power 600 CW-Nd:YAG laser. The hardness depth of hardened layer as well as its microstructure were found to largely depend on the laser scanning speed.
2. At low scanning speeds of 25 cm/min, the surface layer was melted and then solidified at very high cooling rates. The microstructure of the hardened layer consisted mainly of carbides in a matrix of retained austenite and martensite.
3. As the scanning speed increased to 125 cm/min, the hardened surface did not reach the melting point and the austenite formed during heating was transformed to martensite.
4. The rapidly solidified carbidic structure with the low scanning speed of the underlying laser melted track experienced very accelerated graphitisation during the multipass overlap remelting process. Such accelerated graphitisation resulted in the formation of ultrafine graphite nodules and was related to thermodynamic, kinetic factors as well as increased level of crystal defects at the carbide/matrix interface.
5. Some interesting microstructural features were observed at the transition zone between the hardened zone at the HAZ such as the formation of coarse martensite plates and the formation of austenitic/martensitic double layer around the graphite spheroids. Mechanisms were suggested for those structural formations.

References

1. J. Kusinski, S. Kac, A. Kopia, A. Radziszewska, M. Rozmus-Gomkowska, B. Major, L. Major, J. Marczak and A. Lisiecki: Bulletin of the Polish Academy of Sciences, Technical Sciences, 2012, vol. 60, No. 4, 711-728.
2. S. S. Bhavikatti, S. S. Pardeshi and P. K. Mishra: International Journal of Engineering and Innovative Technology (IJEIT), 2012, vol. 2, Issue 2, 42-46.
3. W. A. Monteiro, E. M. R. Silva and W. de Rossi: 3rd International Conference on Integrity, Reliability and Failure, Porto/Portugal, July 2009, Paper Ref: S2403_P0409.
4. H. Matsuyana and K. Shibata: 8th International Congress on Heat Treatment of Materials, Heat and Surface, Kyoto, Japan, 1992, 2207-210.
5. C. H. Chen, C. J. Altstetter and J. M. Rigsbee: Metall. Trans. A, 1984, 719-728.
6. C. H. Chen, C. P. Ju and J. M. Rigsbee: Mater. Sci. Technol, 1988, 4, 161-166.
7. A. Fernández-Vicente, M. Pellizzari and J. L. Arias: Journal of Materials Processing Technology, 2012, 212, 989-1002.
8. D. Farias, S. Denis, A. Simon, Suardi, G. Vinsaro, J. C. Cherrier, J. Quesada, D. Boisselier, A. Cornet and Y. Pourprix: Second International Seminar of Surface Engineering with High Energy Beams, CEMUL (INIC), Lisbon (Portugal), September 25-27, 1989.
9. H. M. Wang and H. W. Bergmann: Metallurgical and Materials Transactions A, April 1995, Vol. 26 A, 793-800.
10. H. M. Wang and H.W. Bergmann: Scripta Metallurgica et Materialia, 1995, vol. 32, No. 8, 1147-1152.

11. C. H. Chen, C. P. Ju and J. M. Rigsbee: Mater. Sci. Technol., 1988, 4, 161-166.
12. C. H. Chen, C. J. Altstetter and J. M. Rigsbee: Metall. Trans. A, 1984, 15, 719-728.
13. J. Grum: In: G. E. Totten, K. Funatani, L. Xie (Eds.) Handbook of Metallurgical Process Design, 2004, Marcel Dekker Inc., New York, 659.
14. J. Grum and R. Sturm: J. Mater. Process. Technol, 2004, 147, 351-358.
15. J. Grum and R. Strum: International Journal of Microstructure Material Properties, 2005, 1(1), 11-23.
16. Y. Chen, C. H. Can, L. X. Wang, G. Yu and A. Kaplan: Applied Surface Science, 2005, 245, 316-321.
17. K. F. Alabeedi, J. H. Abboud and K. Y. Benyounis: Wear, 2009, 266, 925-933.
18. A. K. Mahmoud and M. Mohamed: Machines, Technologies, Materials, 2013, 12, 3-6.
19. M. S. F. Lima and H. Goldenstein: Journal of Crystal Growth, 2000, 208, 709-716.